USE OF AC IMPEDANCE ANALYSIS TO STUDY MEMBRANE CHANGES RELATED TO ACID SECRETION IN AMPHIBIAN GASTRIC MUCOSA

CHRIS CLAUSEN
Department of Physiology and Biophysics, Health Sciences Center, State University of New York Stony Brook, New York 11794

TERRY E. MACHEN
Department of Physiology-Anatomy, University of California, Berkeley, California 94727

JARED M. DIAMOND
Department of Physiology, University of California at Los Angeles School of Medicine, Los Angeles, California 90024

ABSTRACT We have applied transepithelial AC impedance techniques to gastric mucosa to reconcile ultrastructural and electrophysiological findings about gastric acid secretion and the mucosal barrier. By fitting impedance data measured at different HCl secretion rates to equivalent circuit models, we extracted capacitances and resistances (as measures of membrane area and ionic conductance, respectively) for the apical and basolateral membranes. The impedance measurements were found to be incompatible with earlier equivalent circuit models that modeled membrane electrical properties as lumped circuits based on one or two cell types. A distributed circuit model was developed that assumed only one dominant electrical pathway (i.e., one cell type), but that incorporated electrical effects arising from long and narrow membrane-lined structures present in the epithelium (e.g., gastric crypts, tubulovesicles, lateral intercellular spaces). This morphologically based model was found to represent the measured data accurately, and to yield values for membrane capacitances consistent with morphometric measurements of membrane areas. The main physiological conclusions from this analysis were as follows: (*a*) The dominant transepithelial current pathway may reside in the oxyntic cells. (*b*) The transepithelial conductance increase associated with the onset of acid secretion is entirely due to increased conductance of the apical membrane. This is in turn due entirely to increased area of this membrane, resulting from incorporation of tubulovesicular membrane. (*c*) When membrane conductances are normalized to actual membrane area by use of membrane capacitances, it turns out that acid secretion is not associated with a change in specific ionic conductance (change in conductance per unit area) at either the apical or basolateral membrane. (*d*) The puzzlingly low value of transepithelial resistance ($\leq$400 Ω-cm^2) arises because there are hundreds or thousands of square centimeters of actual membrane area per square centimeter chamber area. Apical membrane resistance is 25 kΩ-cm^2 (actual membrane area), implying a tight barrier to back-diffusion of protons.

INTRODUCTION

Amphibian gastric mucosa exhibits two major transport processes that normally appear independent: isotonic HCl secretion, and a separate chloride secretory mechanism that generates a short-circuit current (I_{sc}) (see Machen and Forte, 1979, and Diamond and Machen, 1983). HCl secretion can be modulated independently of I_{sc} by several agents, notably serosally applied histamine, which is thought to stimulate HCl secretion via a common pathway involving increased adenylate cyclase activity of parietal cells and activation of a protein kinase.

Secretagogues like histamine have two further effects whose relation to HCl secretion is not obvious: they cause a dramatic decrease in transepithelial resistance (R_t) and a proliferation of apical membrane area. Rehm (1958) interpreted the drop in R_t (increase in conductance) associated with the onset of acid secretion as a specific increase in membrane permeability coefficients for H^+ and/or Cl^-. He formulated an electrogenic model of HCl secretion in which changes in these membrane permeabilities to H^+ and Cl^- were the ultimate regulators of secretion of these ions. However, micrographic observations in amphibian (Helander et al., 1972) and mammalian (Forte et al., 1975) gastric mucosa show that the parietal cells possess a complex network of membrane structures termed tubulovesicles, some of which penetrate the apical surface and appear to be open to the mucosal solution. On stimulation of HCl secretion, these structures most likely fuse with the

apical membrane and increase its area severalfold; on removal of the stimulus to secretion, this added apical membrane is reclaimed into the intracellular tubulovesicles. These observations prompted Forte et al. (1977) to propose a membrane recycling mechanism that might be involved in the regulation of HCl secretion. According to this model (see also Logsdon and Machen, 1982*b*; Forte et al., 1982), the resistance decrease on onset of acid secretion might reflect solely an increase in the area of apical membrane with unchanged specific permeability properties, rather than the specific permeability changes proposed in the formulation of the electrogenic model.

A further puzzle posed by gastric resistance involves the gastric mucosal barrier: the ability of the mucosa to withstand a steep proton gradient between the stomach lumen (pH ~1) and the serosal bathing solution and blood (pH ~7), suggesting very low permeability to H^+. Most other epithelia capable of maintaining steep ionic gradients have high transepithelial resistance R_t (low ionic conductance). For example, mammalian urinary bladder, which maintains steep ionic gradients between urine and blood, possesses an R_t of up to ~50 kΩ–cm^2 (Lewis and Diamond, 1976). However, the resistance of gastric mucosa is only ~20–400 Ω–cm^2 (Rehm, 1958; Forte and Machen, 1975; McLennan et al., 1980; Raphael and Machen, unpublished observations), a range typical of leaky epithelia that do not maintain such steep gradients (Diamond, 1977). How can gastric mucosa maintain such a tight barrier to H^+ despite such a low resistance? Does the low resistance reflect selective high permeability to other ions (e.g., Cl^-) despite low H^+ permeability? Or could it simply reflect the great proliferation of membrane area due to membrane folding at several levels? (Mammalian urinary bladder, in contrast to gastric mucosa, is a nearly planar and scarcely folded epithelium.)

Prompted by these unsolved problems in the relation of gastric ultrastructure to electrophysiology, this paper addresses the following basic questions: (*a*) What are the separate ionic conductances of the apical and basolateral membranes? (*b*) How do these membrane conductances change from the resting to the HCl-secreting states? (*c*) What are the absolute and relative areas of the apical and basolateral membranes? How do the observed changes in these membrane areas correlate with the HCl secretion process? (*d*) How can the paradox of a low transepithelial resistance despite an effective gastric mucosal barrier be resolved?

Investigators interested in such questions have used equivalent circuit techniques to determine the specific membrane resistances (proportional to the ionic conductances and permeabilities) and membrane electrical capacitances (as measures of membrane areas). The epithelium is modeled as an equivalent circuit composed of resistors and capacitors as analogues of membrane ionic conductances and capacitances respectively. Between 1945 and 1976 six valuable papers carried out equivalent circuit impedance analysis of gastric mucosa by either of two methods: applying alternating-current (AC) frequencies sequentially (Teorell and Wersäll, 1945; Flemström, 1971), or else in effect applying all frequencies simultaneously by measuring the voltage response to applied steps of constant current (Teorell, 1946; Noyes and Rehm, 1970; Wright, 1974; Rehm et al., 1976) (see Diamond and Machen, 1983, for review of impedance analysis in epithelia and its applications to gastric mucosa). In recent years the power of epithelial impedance analysis has been greatly extended by use of morphologically realistic models incorporating distributed resistors, recognition of the drawbacks of the step-response method for detecting distributed resistors, and improved curve-fitting techniques (Clausen et al., 1979; Ring and Sandblom, 1980; Frömter et al., 1981; Clausen and Wills, 1981). Hence we have used meaurements by the AC method to reexamine the equivalent circuit models proposed previously to represent the transepithelial current pathways across gastric mucosa. We then propose a new model derived directly from morphological data on gastric mucosa and supported by the electrical data. Finally, we use this new model to address the above-mentioned basic questions about gastric mucosa and its HCl secretory process. Preliminary reports of these results have been given by Machen et al. (1977) and by Clausen et al. (1982).

METHODS

Tissue Dissection and Mounting

Bullfrog (*Rana catesbiana*) gastric mucosa at room temperature was used in all experiments. The mucosa from the fundic region of the stomach was separated from the muscularis by careful blunt dissection. The tissue was then fastened across a mounting ring fitting into a modified Ussing chamber that virtually eliminated edge damage (see Lewis and Diamond, 1976, for details of the chamber design). Nominal exposed tissue area was 2 cm^2, and each bath contained a solution volume of 15 ml. The chamber permitted continuous pH regulation and oxygenation by well-gassed baths that were gently stirred continuously by the use of magnetic fleas.

Solution Compositions

The serosal (nutrient) solution had the following composition (in millimoles per liter): 86 NaCl, 5 KCl, 1 $MgCl_2$, 1 $CaCl_2$, 18 $NaHCO_3$, 1 NaH_2PO_4, and 10 dextrose. pH was maintained at 7.3 by bubbling continuously with humidified 95% O_2/5% CO_2.

The mucosal (secretory) solution consisted of unbuffered 120 mM NaCl, bubbled continuously by 95% O_2/5% CO_2.

HCl secretion was stimulated by 10^{-4} M histamine-HCl added to the serosal solution. In some cases, it was further enhanced by 5 mM theophylline and/or 5 mM dibutyryl-cAMP. Secretion was inhibited by washing with histamine-free solution, coupled with serosal addition of 10^{-4} M cimetidine (kindly provided by SmithKline and French Labs, Philadelphia, PA).

Measurement of HCl Secretion Rate

The HCl secretion rate was monitored continuously by a pH electrode in the mucosal bath, connected to an automatic recording titrator. The titrator was adjusted to maintain the mucosal pH at 5.0 by addition of

microliter aliquots of a 50 mM NaOH titrant solution, made isosmotic with NaCl.

Electrical Measurements

Transepithelial voltages were measured differentially by a high speed instrumentation amplifier with high ($>10^9\ \Omega$) input impedance. Voltage electrodes, mounted close to the tissue, consisted of either Ag/AgCl wires or else 2.5 M KCl agar salt bridges connected to Ag/AgCl wires. When bridges were used, the bath solutions were changed frequently to avoid KCl build-up in the bath. Current was passed transepithelially with a different set of Ag/AgCl electrodes mounted at opposite ends of the baths, and was measured by a high-speed operational-amplifier current-to-voltage circuit.

The transepithelial impedance was measured in the range of 1 Hz to 10 kHz. Six points were taken per decade of frequency, with repeat points at 10, 10^2, 10^3, and 10^4 Hz measured after each run in order to verify stability of the tissue. Approximately 12 min were needed to acquire all 29 frequency measurements. Sinusoidal constant current was generated by a signal generator (model 4100, Krohn-Hite Corp., Avon, MA), using a series 0.1–1.0 MΩ carbon resistor. Current amplitude was adjusted so that the maximum transepithelial voltage deflection was <5 mV rms.

The transepithelial voltage response was measured by a dual-phase phase-lock amplifier (model 9502, Ortec, Inc., Oak Ridge, TN), which measured the in-phase (real) and quadrature (imaginary) voltages with respect to the sinusoidal current. The gain of the phase-lock amplifier was adjusted at each frequency to provide 3½-digit precision, measured on digital panel meters. The real and imaginary parts of the impedances were computed and subsequently converted to phase angles and Log magnitude.

Corrections were made for two sources of experimental error. First, the preamplifier and chamber exhibit small phase-angle errors (<10° at low and high frequencies, and typically <1° at middle frequencies) due to stray capacitance in the bath, electrodes, and preamplifier, and also due to AC coupling errors in the phase-lock amplifier. In addition, the gain of the preamplifier was found to depend slightly on frequency. Hence, after each experiment the tissue was removed, the chamber was reassembled and filled with 120 mM NaCl, and a calibration run was made. The phase errors were found to be additive and were subsequently subtracted from the experimental phase runs. Similarly, the magnitude data were corrected by dividing the experimental magnitudes by the normalized gain of the calibration run measured at each frequency.

Numerical Analysis of Data

The impedance data consisted of phase angles and impedance magnitudes measured at 29 different frequencies. These data, plotted as a function of frequency, were fitted by equivalent circuit models by means of a curve fitting algorithm that systematically adjusted the model parameters (i.e., resistor and capacitor values) to minimize the sum-square error between the model and the data. As an objective measure of the quality of fit, the Hamilton R-factor (Hamilton, 1964), a statistical parameter related to the F-test, was computed for each fit. Our curve-fitting procedures and statistical tests follow those of Clausen et al. (1979), which should be consulted for details.

THEORETICAL ANALYSIS

The goal of equivalent circuit analysis is to separate and determine the preparation's circuit parameters in order to relate them directly to ionic conductances and capacitances of individual membranes. The capacitances can be used as measures of the true area of a folded membrane since capacitances of biological membranes cluster around 1 $\mu F/cm^2$ of true membrane area (Davson, 1964; Cole, 1972). Critical to the success of this approach is the ability to formulate a morphologically based model circuit composed of resistors and capacitors that correspond analagously

TABLE I
DEFINITION OF SYMBOLS*

	Parameters for lumped one-cell and distributed models	Units
Y_a	Apical membrane admittance ($= G_a + sC_a$)	$ohms^{-1}$
	G_a apical membrane conductance ($= 1/R_a$)	$ohms^{-1}$
	C_a apical membrane capacitance	farads
Y_b	Basolateral membrane admittance ($= G_b + sC_b$)	$ohms^{-1}$
	G_b basolateral membrane conductance ($= 1/R_b$)	$ohms^{-1}$
	C_b basolateral membrane capacitance	farads
R_{ap}	Apical extracellular path resistance	ohms
$R_{ap'}$	Apical intracellular path resistance	ohms
R_{bp}	LIS path resistance	ohms
R_s	Series resistance of unstirred layers	ohms
R_t	Transepithelial resistance	ohms
Z_t	Transepithelial impedance	ohms
s	Laplace transform variable	$seconds^{-1}$
	For sinusoidal steady state, $s = j\omega$, where $\omega = 2\pi \cdot$ frequency (Hz); $j = \sqrt{-1}$	radians · $seconds^{-1}$
$v_t(t)$	Transepithelial voltage response	volts
I_t	Applied transepithelial current amplitude	amperes
τ_a	Apical lumped time constant	seconds
τ_b	Basolateral lumped time constant	seconds
	Parameters for Lumped Two-Cell Model	
Y_a, Y_b	Admittances of first cell type (see above)	$ohms^{-1}$
$Y_{a'}$, $Y_{b'}$	Admittances of second cell type (see above)	$ohms^{-1}$
Y_1, Y_2, Y_3	Composite admittance of simplified lumped two-cell model (see Fig. 1).	$ohms^{-1}$

*Units are for one square centimeter of tissue.

to actual membrane structures. The problems that one faces in performing such analyses are discussed in detail in a recent review (Clausen and Wills, 1981).

Throughout the following discussion the reader should consult the Glossary for definition of symbols used in the equations.

Previous Analyses in Gastric Mucosa

As already mentioned, several investigators have fitted impedance measurements in gastric mucosa and other epithelia to circuit models consisting of so-called lumped (discrete) resistors and capacitors. While these lumped models often provided good fits to data obtained by the step-response method, the sequential-frequency method yielded significant misfits that were treated by ad hoc circuit modifications not corresponding to biological structures, such as nonideal capacitors (Brown and Kastella, 1965), or else addition of a parallel pathway composed of a resistor and capacitor in series (Flemström, 1971). These results suggest that lumped models may be inappropriate for gastric mucosas as for other epithelia. To test this conclusion, our theoretical discussion begins with lumped models.

Lumped Models for Gastric Mucosa

The simplest model for gastric mucosa, a one-cell model, is seen in Fig. 1 *a*. Here, the tissue is assumed to consist of cells that are electrically coupled laterally. The apical and basolateral membranes are each treated as parallel resistor-capacitor (RC) circuits. A small series resistance is also included to represent the finite resistance of the solution filling the unstirred layers of the tissue. No resistor is present in the model to represent the parallel (junctional) conductance, since several lines of evidence indicate that this conductance pathway is insignificant; conservative estimates place its resistance at many times the resistance of the transcellular pathway.[1] The electrical impedance of this circuit is given by

$$Z_t = Y_a^{-1} + Y_b^{-1} + R_s. \quad (1)$$

The voltage response to a step of constant current for this model is given by the sum of two exponential functions:

$$v_t(t) = I_t[R_a(1 - e^{-t/\tau_a}) + R_b(1 - e^{-t/\tau_b}) + R_s]. \quad (2)$$

Noyes and Rehm (1970), Rehm and Tarvin (1978), and Tarvin et al. (1979) have suggested that Fig. 1 *a* may not be a realistic representation of the tissue. They found that Eq. 2 was not fully adequate to fit the measured data; at least a third exponential function was required. Because frog gastric mucosa consists of basically two different cell types—the oxyntic cells and surface cells, each comprising roughly 50% of the cell population (Helander et al., 1972)—incomplete electrical coupling between these cell types could result in a more complicated voltage response than predicted by Eq. 2. Coupling between these cell types is at least conceivable, since it has been observed between other cell types (e.g., Flagg-Newton and Loewenstein, 1980). Cell-to-cell lateral coupling has been observed in *Necturus* gastric mucosa between neighboring surface epithelial cells (Spenney et al., 1974) and also between tubular cells, presumably oxyntic cells (Blum et al., 1972). However, coupling that connects surface epithelial cells to oxyntic cells has not been demonstrated, and recent experiments by Hersey et al. (1982) seem to argue against its existence. Incomplete or absent coupling between cell types would indicate that a more realistic equivalent circuit may require modeling two cell types (Fig. 1 *b*) and would have an electrical impedance given by

$$Z_t = \left[\frac{Y_a Y_b}{Y_a + Y_b} + \frac{Y'_a Y'_b}{Y'_a + Y'_b}\right]^{-1} + R_s. \quad (3)$$

Although Eq. 3 is described by nine circuit elements (resistor and capacitor values for each of the two membranes of each of the two cell types, plus a series resistance), network synthesis techniques (Ruston and Bordogna, 1966, ch. 3) show that the properties of the circuit of Fig. 1 *b* are completely described by the simpler seven-element circuit of Fig. 1 *c*, with impedance given by

$$Z_t = Y_1^{-1} + Y_2^{-1} + Y_3^{-1} + R_s. \quad (4)$$

The step response of the circuit shown in Fig. 1 *c*, determined from the impedance (cf. Eq. 4), consists of the sum of three exponential functions. Because Noyes and Rehm (1970) observed an apparent third exponential in their step measurements, this would yield support for their lumped two-cell model. Unfortunately, the resulting circuit no longer corresponds analogously or morphologically to individual structures of the tissue. Each of the circuit elements of Fig. 1 *c* is instead a complicated function of the elements of Fig. 1 *b*, which do correspond to actual individual structure.

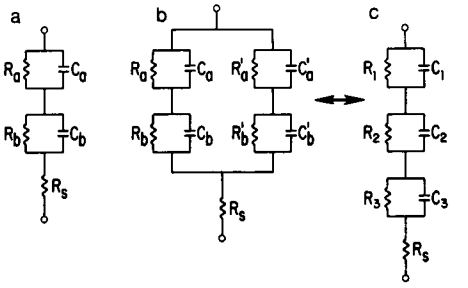

FIGURE 1 (*a*) Schematic representation of the lumped one-cell model. The apical and basolateral membranes are represented as discrete (lumped) parallel RC circuit elements. The series resistance R_s represents the resistance of the bathing solution in the unstirred layers on both sides of the tissue; from transepithelial measurements, R_s appears as a single-circuit element. (*b*) Schematic representation of the lumped two-cell model, which differs from the lumped one-cell model in that the two major cell types of the tissue are considered electrically isolated (due to poor lateral coupling) and in parallel with each other. (*c*) The lumped two-cell model of Fig. 1 *b* consists of nine circuit elements, but reduces mathematically to this simpler model. It consists of seven parameters that have lost their one-to-one correspondence with actual membrane resistors and capacitors (see section on Distributed Model of Gastric Macosa). See Table I for description of the symbols.

Distributed Model of Gastric Mucosa

Clausen et al. (1979) and Clausen and Wills (1981) showed that the geometry of the tissue requires special consideration when determining an equivalent circuit model for an epithelium. Infolded membrane structures like the narrow lateral intercellular spaces (LIS) in mammalian urinary bladder, or like the deep crypts in mammalian descending colon, behave

[1]Four lines of evidence indicate that the conductance of the paracellular (junctional) pathway in frog gastric mucosa is negligible: (*a*) As in epithelia known to have tight junctions, active transport in gastric mucosa supports a large transepithelial potential when the tissue separates identical solutions (~30 mV, Rehm and Sanders, 1972). In contrast, potentials across leaky epithelia separating identical solutions rarely exceed a few millivolts (Frömter and Diamond, 1972). (*b*) By means of microelectrode cable analysis techniques, Spenney et al. (1974) showed that the paracellular shunt conductance was at most only 25% of the transcellular conductance. (*c*) Using a sodium backflux technique, Machen et al. (1978) estimated that ~20% of the transepithelial conductance could be accounted for by the paracellular junctional pathway. Because of edge-damage artifacts, this estimate and that of Spenney et al. should be taken only as upper limits. (*d*) Gastric mucosa is capable of supporting an enormous proton gradient (10^6:1), which one would expect to be rapidly dissipated if paracellular conductance were significant.

as distributed resistors, producing effects observable in the measured impedance of these tissues. These effects arise from the significant series resistance caused by the narrowness of these membrane-lined paths. Lumped models neglect these effects and result in poor fits of the model to measured data. In addition, Clausen et al. (1979) found that lumped models systematically underestimate the capacitance of an infolded membrane.

An equally important outcome of the analysis of epithelial impedance by distributed models was that it enabled these authors to obtain morphological information from electrical measurements alone. In the case of mammalian urinary bladder, the LIS width could be determined by fitting a distributed model to measured impedance data (coupled with light microscopic measurements of average cell dimension), and the values thus determined agreed well with those obtained from electron microscopic observations of fixed tissues.

A priori, distributed effects should be even more important in gastric mucosa than in rabbit urinary bladder or colon, because membrane folding at several levels is much more conspicuous in gastric mucosa. The already mentioned deviations of impedance data from predictions based on lumped models might simply be due to distributed effects arising in one electrically dominant cell type. This membrane folding is expected not only to cause distributed effects, but also to amplify the true membrane area of the tissue by a large and unknown factor, possibly by one or more orders of magnitude. In addition, membrane elaboration by tubulovesicles at the apical membrane of the oxyntic cells might cause their membrane area and conductance to be so high that this cell type would constitute the major transepithelial ionic pathway across the mucosa. Hence the electrical properties of the mucosa might be dominated by oxyntic cell properties, and a one-cell distributed model might be adequate to represent the electrical properties of the epithelium.

The Distributed Impedance at the Apical Membrane of the Oxyntic Cells

Distributed effects arise when the series path resistance of a membrane-lined structure becomes comparable to the transmembrane impedance. At the apical surface of gastric mucosa, distributed effects could arise from two structures: the narrow gastric crypts at the light microscopic level, and the tubulovesicles that penetrate the apical membrane at the electronmicroscopic level. The area-to-length ratio of each of these structures, coupled with the resistivity of the solution filling them, determines this pathway resistance. The penetrating tubulovesicles have diameters of only ~100–500 Å, whereas the diameter of the gastric crypts is several microns. For this reason the path resistance per unit length of tubules will be much higher for the tubules than for the crypts. However, the length of the crypts ($\geq$100 μm) greatly exceeds that of the tubulovesicles (a few micrometers). Thus, it is not clear which of these two structures has the lower area-to-length ratio and is more significant as a distributed resistor. Nevertheless, the theoretical treatment of the distributed effects is similar for these two structures, both of which can be modeled as finite terminated cables (transmission lines) (see Jack et al., 1975, for a detailed discussion of the mathematical analysis).

In the case where the crypt resistance dominates, the model seen in Fig. 2 *a* would be a reasonable representation. The impedance of this model is given by

$$Z_a = \sqrt{R_{ap}/Y_a}\coth\sqrt{R_{ap}Y_a}. \tag{5}$$

Here the parameter R_{ap} is interpreted as the crypt path resistance, and is given by

$$R_{ap} = R\ell/A \tag{6}$$

where R is the resistivity of the solution filling the crypt (Ω–cm), ℓ is the average crypt length (in centimeters), and A is the crypt cross-sectional area (cm^2/cm^2 of tissue).

If, on the other hand, the tubulovesicular resistance dominates, then the model seen in Fig. 2 *b* would be a reasonable representation. The impedance of this model is given by

$$Z_a = \frac{(R_{ap}^2 + R_{ap'}^2)\coth\Gamma + R_{ap}R_{ap'}(\operatorname{csch}\Gamma - \Gamma)}{\Gamma(R_{ap} + R_{ap'})} \tag{7}$$

where

$$\Gamma^2 = Y_a(R_{ap} + R_{ap'}).$$

Here, the tubular extracellular path resistance R_{ap} has an interpretation similar to that for the crypt. However, since microscopic observations (Helander et al., 1972) indicate that the tubules are sometimes observed in densely packed hexagonal arrangements, then the intracellular "antitubular" path would have a resistance ($R_{ap'}$) comparable to the tubular resistance itself. Hence, a "double cable" structure results.

Eq. 7 is significantly more complicated than the single-cable representation of Eq. 5 due to the presence of two different path resistances that must be determined from the impedance data. It is doubtful that impedance measurements would be capable of separating the two path resistances, and for this reason we considered several limiting cases to simplify the model.

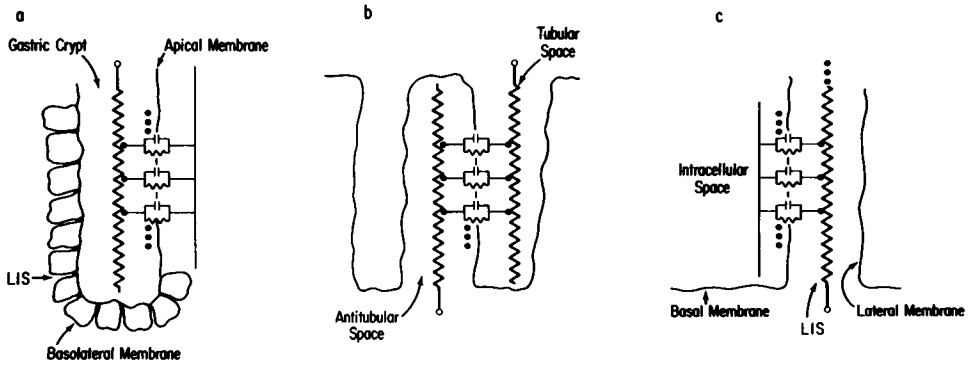

FIGURE 2 Schematic representations of the distributed model apical impedance. (*a*) Here the distributed effects are attributed to the path resistance arising from the narrow gastric crypts. (*b*) Here the distributed effects are attributed to tubulovesicles penetrating the apical surface of the oxyntic cells. The tubules are packed so closely that a double-cable structure results, with extracellular (tubular space) and intracellular (antitubular space) path resistances (see section on the Distributed Impedance at the Apical Membrane of the Oxyntic Cells). (*c*) Schematic representation of the distributed model basolateral impedance. The tortuously long and narrow LIS constitute a distributed path resistance.

Consider the case where one of the two path resistances dominates in magnitude. For example, if the packing of the penetrating tubules were not close, then the resistance of the intracellular antitubular space (basically, intracellular free solution) would be much less than that of the extracellular tabular space (i.e., $R_{ap} \gg R_{ap'}$). Conversely, if the tubules were closely packed and if the resistivity of the intracellular solution were high compared to the extracellular tubular resistivity (e.g., because of lower resistivity of the isotonic HCl presumably filling the tubulovesicles), then the antitubular path resistance would be expected to dominate (i.e., $R_{ap'} \gg R_{ap}$). In either case, Eq. 7 simplifies greatly to the same expression seen in Eq. 5. The interpretation of R_{ap} in Eq. 5, however, would differ from that originally proposed: it would represent either the tubulovesicular path resistance (when $R_{ap} \gg R_{ap'}$) or else the antitubular path resistance (when $R_{ap'} \gg R_{ap}$).

Finally another limiting case can be considered. If $R_{ap} = R_{ap'}$, the impedance of the model of Fig. 2 *b* becomes

$$Z_a = \sqrt{R_{ap}/2Y_a}\,(\operatorname{csch}\sqrt{2R_{ap}Y_a} + \coth\sqrt{2R_{ap}Y_a}) + R_{ap}/2. \quad (8)$$

Due to the symmetry of the double cable, all cases when $R_{ap} \neq R_{ap'}$ will lie somewhere between the two limits (i.e., Eqs. 5 and 8). Moreover, our experience indicates that both these equations produce similar effects in the impedance, and for this reason we arbitrarily chose to use the model representing a single cable (Eq. 5).

The reader should keep in mind that the interpretation of the path resistance R_{ap} differs depending on whether the major distributed effects arise from the crypts, the extracellular tubular resistance, or the intracellular antitubular resistance. The relevant equations are too similar for our measurements to be able to decide which of these three possible sites of apical distributed effect is most important.

Geometric Electrostatic Effects

The capacitance C_a is useful as an estimate of the true area of the apical membrane. However, what area does C_a actually represent? Because the diameter of the tubules (~100 Å) is comparable to the membrane thickness (also ~100 Å), does C_a represent the membrane area determined by the inner or outer tubular radii? If tubules were closely packed at the apical surface of the oxyntic cells, this question would significantly affect the interpretation of the capacitance values.

This question can be addressed by electrostatic theory (see ch. 30 of Halliday and Resnick, 1967, for detailed discussion). Briefly, if one treats the membranes as cylinders of low dielectric constant, bordered by solution of high conductivity, then one calculates that the capacitance of the tubules will be anomalously high by the factor

$$C/C_0 = (d/a)/\log(1 + d/a) \quad (9)$$

where d is the membrane thickness, a is the tubular inner radius, and C_0 is the specific capacitance of the membrane (~1.0 μF/cm^2). In essence, the measured capacitance C_a would be in error by the factor C/C_0 arising from the tubular geometry of the membrane. This error can be significant. If one assumes a membrane thickness of 100 Å, then the measured value for C_a would range from 20 to 420% higher than that predicted for an infinitely thin membrane as the inner tubular radius ranged from 200 down to 10 Å, respectively. This effect is only an anomalous capacitance increase; it does not reflect true surface area.

Actually, this electrostatic treatment is an oversimplification, since it assumes that the tubular and antitubular species are good conductors. In reality, the dense packing of the tubules observed in micrographs is expected to increase this anomalous capacitance still further (A. Peskoff, personal communication). The mathematical analysis necessary to estimate these effects, however, is beyond the scope of this paper.

The Distributed Impedance at the Basolateral Membrane

Clausen et al. (1979) have shown that the LIS of rabbit urinary bladder must also be represented as a distributed impedance when the LIS are narrow (~100 Å) and tortuous (hence long). We treat the basolateral impedance of gastric mucosa in much the same way, as

$$Z_{bl} = \sqrt{R_{bp}/Y_b}\coth\sqrt{R_{bp}Y_b} \quad (10)$$

Note that the equations for the basolateral impedance (Eq. 10) and the apical impedance (Eq. 5) are identical in form. In the basolateral case, R_{bp} is interpreted as the path resistance of the lateral spaces.

The Complete Model

The complete transepithelial equivalent circuit, based on morphological observations of the tissue, is given simply by the series combination of the apical and basolateral impedances (i.e., the sum of Eqs. 5 and 10) coupled with an added small series resistance R_s necessary to represent the resistance of the unstirred layers in the bathing solution. As already discussed (footnote 1), other evidence indicates that the paracellular resistance is severalfold higher than the transcellular impedance and hence can be ignored as a significant pathway for transepithelial ionic current flow.

Note that the complete distributed model contains two more parameters (R_{ap} and R_{bp}), than the lumped one-cell model. These two extra parameters are determined by tissue geometry. The distributed model contains the same number of parameters as the lumped two-cell model of Fig. 1 *c*.

RESULTS

We gathered complete sets of impedance data in six preparations, each at several different HCl secretion rates (cf. Figs. 3–5). Each of the 17 resulting impedance runs was fitted to three circuit models: the lumped one-cell model (Fig. 1 *a* and Eq. 1), the lumped two-cell model (Fig. 1 *c* and Eq. 4), and the distributed model (Fig. 2 *a* and Eqs. 5 and 10). To be regarded as adequate, a model must satisfy two types of criteria: it must fit the measured data accurately, without systematic misfits; and the extracted values of circuit parameters must agree with values obtained by other methods (e.g., the capacitance values must be compatible with membrane areas measured from electron micrographs by morphometric techniques).

Analysis by the Lumped One-Cell Model

This is the simplest of the three models. Fig. 3 illustrates typical fits of this model to two different impedance runs in the same preparation, one at low and the other at high acid secretion rates.

In these two runs as in all others, there is significant disagreement between measured impedances and the best fit obtained by the lumped one-cell model. For all 17 runs the average percent error of fit, reflected in the R-factor statistic, was 7.1 ± 0.4% (average ± SEM). Note in Fig. 3 that this error does not appear to be due to random experimental errors in the impedance measurements. Instead, there are systematic misfits that appear as wiggles

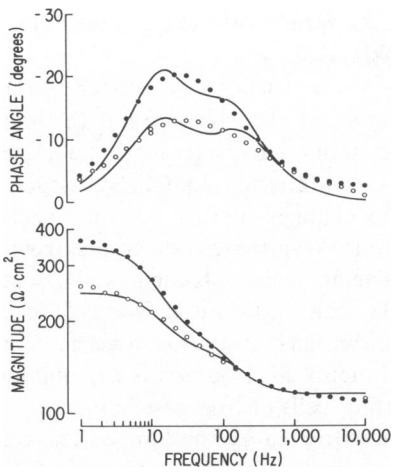

FIGURE 3 Fits of lumped one-cell model to measured impedance. The upper curves show the phase angle response, and the lower curves show the magnitude of the impedance (logarithmic scale). Symbols are measured data; solid lines are the fit by the model. The deviations between the fitted curves and the data illustrate the inability of the model to fit the measured data. ●, data from a nonsecreting tissue (run 3-2, Table II). Best-fit model parameters, R_a = 170 Ω-cm², C_a = 100 μF/cm², R_b = 58 Ω-cm², C_b = 25 μF/cm², R_s = 120 Ω-cm²; R-factor = 6.9%. O, data from the same tissue after secretion has been stimulated by 10^{-4} M serosal histamine (run 3-3, Table I). Best-fit model parameters, R_a = 88 Ω-cm², C_a = 170 μF/cm², R_b = 44 Ω-cm², C_b = 23 μF/cm², R_s = 120 Ω-cm²; R-factor = 8.7%.

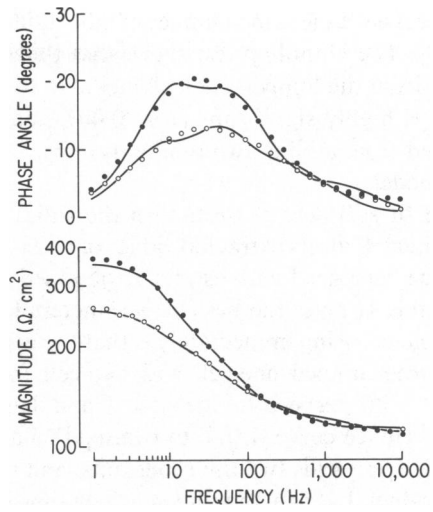

FIGURE 4 Fits of the lumped two-cell model to the same points as shown in Fig. 3. Although the deviation of the data points from the fitted curve is less than for the lumped one-cell model (Fig. 3), the deviations show clear trends that are not observed in the data and that cannot be explained by random measuring errors. Best-fit model parameters (●, nonsecreting tissue), R_1 = 160 Ω-cm², C_1 = 130 μF/cm², R_2 = 72 Ω-cm², C_2 = 36 μF/cm², R_3 = 14 Ω-cm², C_3 = 6.5 μF/cm², R_s = 110 Ω-cm²; R-factor = 3.7%. Best-fit model parameters (O, secreting tissue), R_1 = 64 Ω-cm², C_1 = 440 μF/cm², R_2 = 58 Ω-cm², C_2 = 65 μF/cm², R_3 = 22 Ω-cm², C_3 = 16 μF/cm², R_s = 110 Ω-cm²; R-factor = 4.3%.

in the best-fit curves. As in rabbit urinary bladder (Clausen et al., 1979), the misfits are more noticeable for the phase-angle measurements than for the magnitude measurements. We therefore agree with the conclusion of Noyes and Rehm (1970) and of Rehm and Tarvin (1978) that the lumped one-cell model is inadequate to represent accurately the transepithelial current pathways across gastric mucosa. Hence we reject it as an equivalent circuit model and will draw no further conclusions from it.

Analysis by the Lumped Two-Cell Model

This model was originally proposed by Rehm and colleagues to explain deviations from the lumped one-cell model as seen in data gathered by the step-response method. Fig. 4 illustrates fits by this model to the same data as were fitted to the lumped one-cell model in Fig. 3. Clearly, in part because the lumped two-cell model has two more adjustable parameters than the lumped one-cell model, there is a dramatic reduction in the disagreement between measured impedances and the best-fit curve, and this is reflected in a reduced percent error (mean R-factor) of 4.2 ± 0.2% (n = 17). However, one still observes systematic misfits between the measurements and the best-fit curve in Fig. 4 as in all other experimental runs. Therefore, the hypothesis that deviations from the lumped one-cell model are explained by the presence of two-cell types can be rejected.

Analysis by the Distributed Model

Fig. 5 shows the fit of the distributed model to the same data as were fitted to the other two models in Figs. 3 and 4. Observe that the resulting agreement between the best-fit curve and the measured data is significantly improved; the mean R-factor by this model is reduced to 2.8 ± 0.3% (n = 17). Notice also that the systematic misfits or wiggles seen in the fits by the lumped one-cell and two-cell models are gone, even though the distributed model and the lumped

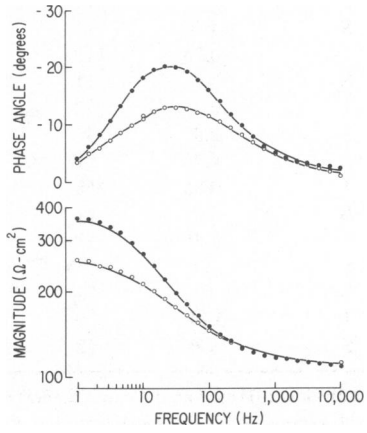

FIGURE 5 Fits of the distributed model to the same data points as shown in Figs. 3 and 4. Note the good fits: the clear deviations that were observed in fits by the lumped one-cell model (Fig. 3) and the lumped two-cell model (Fig. 4) are absent for the distributed model. For best-fit parameter values, see Table II, runs 3-2 (●) and 3-3 (O).

two-cell model have the same number of adjustable parameters (seven). The Hamilton test shows that the improved fit on going from the lumped one-cell model to the distributed model is highly significant ($p \ll 0.001$), not merely that expected from adding two randomly chosen parameters to the model.

The good fit still does not establish the validity of the distributed model, for its extracted values of circuit parameters must be compared with estimates obtained by other methods. Table II gives the best-fit parameters for all 17 runs. A problem arising immediately is that the distributed model, like the lumped one-cell and two-cell models, is symmetrical with respect to the apical and basolateral membranes. Hence curve fitting to transepithelially measured impedances yields two time constants, and two pairs of R and C values, but cannot indicate which time constant applies to which of the two membranes: additional independent information is needed to answer this question. We used two types of reasoning to make this assignment.

First, we noted that the higher of the two extracted capacitance values (the one associated with the longer time constant) increased with J_{H^+} (acid secretion rate), but the lower of the extracted capacitance values did not vary significantly with J_{H^+}. Electron microscopy shows the transition from the resting to secreting state to be associated with a dramatic increase in apical membrane area but not in basolateral membrane area, and also shows that the apical membrane has the greater area in any state. This implies that the longer time-constant belongs to the apical membrane, as Wright (1974) concluded previously by the same reasoning.

Second, we independently measured the membrane resistance ratio in the nonsecreting (cimetidine-treated) state by means of microelectrodes and obtained $R_a/R_b \sim 4$ (Clausen and Machen, unpublished observations). We observed no changes in this ratio as we advanced the microelectrode down the gastric crypts, from surface cells toward parietal cells. Machen and Zeuthen (1982) obtained the same ratio in surface cells of nonsecreting (cimetidine-treated) *Necturus* gastric mucosa, while Schettino (unpublished observations) obtained R_a/R_b of 5–7 for surface cells of frog gastric mucosa. These R_a/R_b values were extracted by the lumped one-cell model and are therefore contaminated by effects of series resistance and of distributed path resistance. Nevertheless, this uncertainty is very unlikely to affect the qualitative conclusion that $R_a > R_b$. For comparison, our six impedance runs at $J_{H^+} < 1$ μeq/cm^2/h yielded an average value of 2.8 for the resistance of the long–time-constant membrane divided by that of the short–time-constant membrane. This confirms the identification of the long–time-constant membrane as the apical membrane.

On these two bases we identify R and C for the long–time-constant membrane as R_a and C_a (for the apical membrane in Table II), R and C for the short–time-constant membrane as R_b and C_b (for the basolateral membrane).

We used regression analysis and the t-test to examine

TABLE II
PARAMETERS FOR INDIVIDUAL EXPERIMENTS, EXTRACTED FROM DISTRIBUTED MODEL

Run	State	J_{H^+}	R_a	C_a	R_{ap}	R_b	C_b	R_{bp}	R_s	R-fact
1-1	S	na	46	600	22	38	140	2.6	150	2.3
1-2	I	~0.0	150	200	20	30	130	1.9	130	2.7
2-1	B	3.6	18	1,900	16	46	110	15	130	2.8
2-2	S	4.3	11	8,500	8.8	40	120	18	120	2.4
2-3	S	4.2	6.2	20,000	9.2	38	220	22	120	2.3
2-4	I	0.25	110	270	12	50	140	19	110	3.3
3-1	S	3.8	11	2,900	12	60	50	12	110	3.6
3-2	I	0.3	82	420	3.4	30	150	2.4	110	1.5
3-3	S	2.8	32	1,800	19	42	170	16	110	1.8
4-1	B	4.2	5.6	13,000	1.5	16	170	24	130	4.5
4-2	I	0.85	58	170	0.1	26	90	18	130	5.9
5-1	B	2.5	4.6	2,000	56	88	11	15	160	2.3
5-2	I	0.0	18	600	76	86	13	10	150	1.7
5-3	S	2.4	0.9*	26,000*	58	54	26	20	150	3.4
6-1	B	1.9	72	165	28	16	58	3.2	150	2.3
6-2	I	0.24	120	170	30	26	27	3.8	150	1.6
6-3	S	1.6	58	310	30	14	55	4.4	150	2.9

The first column (Run) identifies the actual experimental run; the first number is the tissue number and the second number is the run number (e.g., 1-1 and 1-2 are from the same tissue). The second column gives the state of the tissue: S, acid secretion stimulated by histamine (in some cases further enhanced by theophylline or dibutyryl-cAMP); I, acid secretion inhibited by cimetidine; B, basal acid secretion in the absence of histamine or cimetidine. See Glossary and the text for definition of the parameters. J_{H^+} is the HCl secretion rate (μeq/cm^2/h); R_a and R_b, apical and basolateral membrane resistance (Ω-cm^2); C_a and C_b, apical and basolateral capacitance (μF/cm^2); R_{ap} and R_{bp}, apical and basolateral distributed path resistance (Ω-cm^2); R_s, series resistance (Ω-cm^2). "cm^2" in all these units refers to chamber area. R-fact is the Hamilton R-factor (see section on Numerical Analysis of Data) and gives the percent residual error between the fitted impedance and the measured data. na means that the value was not measured.

*The very high C_a and very low R_a value for run 5-3 are puzzling, considering the modest J_{H^+} value for that run. Because these values lie several standard deviations outside the mean values for runs with $J_{H^+} \geq 3.0$ μeq/cm^2,h, we disregard this run in our discussion of the dependence of R_a and C_a on J_{H^+}.

whether each of the seven extracted parameters varied with J_{H^+}. It turned out that apical capacitance C_a increased with J_{H^+}; apical resistance R_a decreased with J_{H^+}; and basolateral capacitance C_b and resistance R_b, apical and basolateral distributed path resistance R_{ap} and R_{bp} respectively, and series resistance R_s did not vary with J_{H^+} ($p \ll 0.05$ based on the slope of the regression line). Hence average values of the latter five parameters over all values of J_{H^+} were computed.

We now consider the extracted values for each parameter.

Membrane Capacitances

C_b has a mean value of 99 ± 14 μF/cm^2 (n = 17), suggesting 99 cm^2 of basolateral membrane area per cm^2 of chamber area. This value agrees well with the value of 89 cm^2/cm^2 that Helander et al. (1972) determined for basolateral membrane area of frog gastric mucosa oxyntic cells by morphometric analysis of electron micrographs. This 99-fold increase in area over that expressed for a flat sheet arises from folding at four levels: the whole epithelium has gross folds; it is further infolded into gastric crypts; the basolateral membrane would have five times the area of the apical membrane in a cuboidal cell; and the lateral spaces are not smooth but tortuous.

The lumped model yielded an average C_b value of only 17 ± 3 μF/cm^2 (n = 17). The reason for this underestimation is that the distributed resistance of the lateral spaces is in series with the lateral part of the basolateral membrane. Ignoring this distributed resistance by using a lumped model effectively reduces the basolateral membrane area available for current flow. Use of a lumped model similarly underestimates C_b in rabbit urinary bladder, though by a smaller factor (Clausen et al., 1979).

Apical capacitance C_a increases 100-fold from 200 to 20,000 μF/cm^2 with increasing HCl secretion rate (Fig. 6). An increase was seen in each individual preparation studied. The explanation is the increase in apical membrane area that electron microscopy has documented in the secreting preparation, due to fusion of tubulovesicles into the apical membrane (Forte et al., 1972; Helander et al., 1972). Helander et al. reported 188 cm^2 of oxyntic cell apical membrane per cm^2 chamber area for tissue removed directly from the animal. These authors did not measure HCl secretion rates, but we assume that their tissues were secreting at a modest rate (we find significant HCl secretion at 3.0 ± 0.5 μeq/cm^2/h [n = 4] in the resting mucosa). The morphometric value of 188 cm^2/cm^2 is below the lower end of our range (~200 – 20,000 cm^2/cm^2 on the assumption that 1 μF ~ 1 cm^2). However, the morphometric value is an underestimation because Helander et al. (1972) could not know which tubulovesicles were open to the mucosal solution and therefore did not count tubulovesicle area.

We suspect that the abrupt increase in C_a at high secretion rates above 3.5 μeq/cm^2/h does not reflect a true increase in area but instead an anomalous capacitance increase due to tubular close packing or constricted radii, as discussed above (section on Geometric Electrostatic effects). This effect may also explain the 100-fold increase in C_a with stimulation compared to the 6–10-fold increase measured morphometrically on micrographs (Logsdon and Machen, 1982*a*).

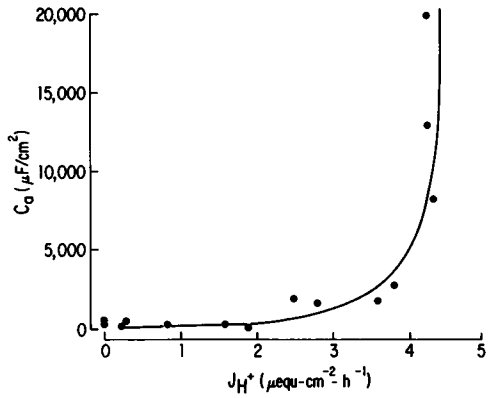

FIGURE 6 Apical capacitance (●) determined from fits by the distributed model, plotted as a function of HCl secretion rate (J_{H^+}). Values are from Table II, omitting runs 1-1 (J_{H^+} not measured) and 5-3 (see Table II legend for explanation). The line is drawn by eye and is intended only to emphasize the trend in the data.

Membrane Resistance Relative to Chamber Area

Expressed relative to chamber area, R_b is 41 ± 5 Ω–cm^2 (n = 17) independent of HCl secretion rate. R_a decreases from 150 to 4.6 Ω–cm^2 with increasing secretion rate. These R_b and R_a values are both absurdly low compared with values for other epithelia that do not exhibit such enormous proliferation of membrane area (e.g., gallbladder and rabbit urinary bladder). This discrepancy could be due to the stomach's proliferation of area, and the increase of apical membrane area with secretion could similarly explain the decrease in R_a with secretion. Hence we next calculated membrane resistances relative to membrane capacitances as a measure of true membrane area.

Membrane Resistances Normalized to Membrane Capacitance

Resistances normalized for membrane area are computed as the product of the membrane resistance and the corresponding capacitance and are expressed in units of ohms · microfarads (i.e., R_a-norm = R_aC_a; R_b-norm = R_bC_b). R_b-norm is 3.5 ± 0.6 KΩ–μF (n = 17), and R_a-norm is 25 ± 4 kΩ–μF (n = 14) (the latter calculation omits values above J_{H^+} = 3.5 μeq/cm^2/h, where we suspect that C_a is inflated by electrostatic effects). Both R_b-norm and R_a-norm are independent of secretion rate. Thus, the decrease in R_a with secretion rate is due entirely to the increase in apical membrane area; these R_b-norm and R_a-norm values are typical of those for other transporting epithelia. For

instance, the corresponding values for rabbit urinary bladder are 8 and 10–80 kΩ–μF, respectively (Lewis and Diamond, 1976; Clausen et al., 1976).

Distributed Path Resistances

R_{ap}, the distributed path resistance at the apical membrane, has a mean value of 24 ± 5 Ω–cm^2 (n = 17). A priori, we did not know whether R_{ap} would be dominated by the resistance of the solution filling the crypts, the extracellular tubular space, or the intracellular antitubular space. However, in rabbit descending colon, which has crypts but no tubules, R_{ap} has a similar value (17 Ω–cm^2), which is in accord with the value expected from the dimensions of the crypts in that epithelium (Clausen and Wills, 1981). This suggests that the R_{ap} value of gastric mucosa may also be dominated by the crypts. In accord with this interpretation, R_{ap} is independent of HCl secretion rate, whereas one might expect it to vary with secretion if it arose from the tubules or antitubles, since their morphology varies greatly with secretion.

The basolateral path resistance R_{bp}, which we interpret as arising in the lateral spaces, is 12 ± 2 Ω–cm^2 (n = 17) and is independent of secretion rate. Since the ratio of R_{bp} to R_b is much higher in gastric mucosa (12/41) than in rabbit urinary bladder (11/6300, calculated from data in Clausen et al., 1979), we expect distributed effects at the basolateral membrane to be much more serious in gastric mucosa than in rabbit urinary bladder. This is true: Use of the lumped model underestimates C_b by 24% in rabbit urinary bladder, but by 83% in gastric mucosa.

Series Resistance

R_s, the series resistance between the voltage-measuring electrodes and the cell membranes, is 130 ± 4 Ω–cm^2 (n = 17). With the preparation removed, the resistance between the two electrodes is only 40 Ω–cm^2. Hence the connective tissue must restrict diffusion more than does an equivalent thickness of free solution.

DISCUSSION

Choice of Circuit Model

The lumped two-cell model previously appeared adequate to fit impedance measurements on gastric mucosa (Noyes and Rehm, 1970; Rehm et al., 1976; Rehm and Tarvin, 1978). In retrospect, the reason for its apparent adequacy is now seen to be the use of step-response measurements to gather impedance data. We have shown elsewhere, by studies of simulated circuits with parameter values in the physiological range for epithelia, that step-response analysis is unable to recognize epithelial distributed resistors (Clausen et al., 1979). This is because effects of distributed resistors appear at middle to high frequency, whereas an applied step of constant current weights low frequencies. Thus, for gastric mucosa, the lumped two-cell model fits step-response data well, but gives a poor fit to data obtained by applying frequencies sequentially. In addition, the value for C_b extracted by the lumped two-cell model is 83% below what we believe to be the correct value, as extracted by the distributed model and validated by morphological data.

The distributed model gives a good fit to measured impedances, and yields parameter values consistent with other types of data. This success is pleasing but initially puzzling: the distributed model is a one-cell model, yet bullfrog gastric mucosa has two major cell types. We suggest two alternative explanations for this paradox. First, it remains uncertain whether there is lateral coupling between oxyntic cells and surface epithelial cells. If there were, a one-cell model would be valid, with extracted parameter values representing weighted averages of values of the two cell types. Second, the apical membrane area of the oxyntic cells is at least one and possibly two orders of magnitude greater than that of the surface epithelial cells. Morphometric estimates are 188 and 23 cm^2 membrane/cm^2 chamber, respectively (Helander et al., 1972), and the former value is an underestimation for reasons already discussed. Thus, the oxyntic cells probably provide at least 90% of the transepithelial conductance, and the effect of the second cell type might not be detectable in transepithelial impedance measurements. Consistent with this conclusion is the fact that the basolateral membrane area estimated for gastric mucosa by transepithelial impedance measurements (99 cm^2/cm^2) is close to the morphometric estimate for the basolateral membrane area of the oxyntic cells alone (89 cm^2/cm^2).

Parameter Values

We can now use the parameter values extracted by the distributed model to reassess the basic questions about gastric acid secretion posed in the introduction:

The very high membrane capacitances of gastric mucosa reflect the high degree of membrane folding, as Noyes and Rehm (1970) and Wright (1974) concluded previously in their pioneering studies of this preparation.

The decrease in gastric resistance with onset of acid secretion is due solely to a drastic decrease in apical membrane resistance. This latter decrease is in turn due solely to a drastic increase in apical membrane area, as a result of incorporation of tubulovesicular membrane. There appears to be no change in apical membrane conductance per unit of membrane area.

The paradox that gastric mucosa exhibits a transepithelial resistance in the range for leaky epithelia but otherwise behaves like a tight epithelium has a morphological solution. The low resistance simply reflects the fact that the stomach packs hundreds or thousands of square centimeters of tight cell membranes with tight junctions (especially tight to H^+) into 1 cm^2 of chamber area. Normalized to true membrane area through membrane capacitance, the

resistances of the apical and basolateral membranes are similar to those of other tight epithelia. Although apical membrane resistance is sometimes (at high secretion rates) lower than basolateral membrane resistance when normalized to chamber area, the apical membrane always has the higher resistance when both resistances are normalized to membrane area.

Future Directions

We briefly mention some unsolved problems for the future:

Impedance analysis of gastric mucosa yields five parameters susceptible to morphological interpretation: apical capacitance, basolateral capacitance, apical path resistance, basolateral path resistance, and the anomalous increase in apical capacitance seen at high secretion rate. Potentially, these parameters contain information otherwise obtainable only by morphometric methods, which are subject to the problems of statistical sampling and of fixation-related structural changes inherent in electron microscopy. The morphological information extracted from impedance analysis has the advantage that it applies to the living, unfixed tissue. We have exploited this potential for only the first two of these five parameters, and only for the normal conditions of resting and stimulated. Other conditions exist in which the close relationship between apical membrane conductance and area may not hold, e.g., treatment with SCN^- or with glucose-free solutions (Black et al., 1980). Studying these and other physiological states may yield useful information about the control of conductance pathways in both apical and basal cell membranes.

We remain uncertain about the anatomical interpretation of the apical path resistance. Does it arise from the gastric crypts, the tubules, or the antitubules? The area-to-length ratio for the basolateral distributed path resistance is believed to describe the lateral intercellular spaces. This ratio, as well as that at the apical membrane, would be an important parameter for deciding among competing theories of water transport, which is incompletely understood in gastric mucosa (see Machen and Forte, 1979, for a review).

Recently developed techniques for intracellular impedance analysis (Frömter et al., 1981) may prove useful in separating the properties of the oxyntic cells from those of the surface epithelial cells.

Our procedure of applying AC frequencies sequentially has the disadvantage that ~12 min are required for an impedance run. This is much too slow for following the changes associated with the onset of acid secretion: we can only study the tissue at different steady-state rates of secretion. Recently developed techniques for rapid impedance analysis, using pseudorandom binary noise signals (Clausen and Fernandez, 1981; Clausen and Wils, 1981), may prove to combine the speed of the step-response method with the sensitivity of the sequential frequency method.

Extraction of membrane capacitances by impedance analysis may be helpful in studying other epithelial processes where incorporation of intracellular membrane into a surface membrane is thought to play a role, as in gastric mucosa. Examples include apical membrane incorporation of ADH-stimulated water channels in toad urinary bladder (Wade et al., 1981; Stetson et al., 1982), aldosterone-stimulated Na^+ channels in rabbit urinary bladder (Lewis and Moura, 1982), and H^+ pumps in turtle urinary bladder (Gluck et al., 1982).

We thank Dr. Arthur Pestioff for suggestions.

These studies were supported by National Institutes of Health grants AM 17328 (Center for Ulcer Research and Education), GM 14772, AM 19520, AM 28074.

Received for publication 3 August 1982 and in revised form 16 September 1982.

REFERENCES

Black, J. A., T. M. Forte, and J. G. Forte. 1980. Association and dissociation of ultrastructural change and HCl secretion in the mammalian gastric oxyntic cell. *Fed. Proc.* 39:377*a*.

Blum, A. L., B. I. Hirschowitz, H. F. Helander, and G. Sachs. 1972. Electrical coupling and conductive shunts in Necturus gastric mucosa. *In* Gastric Secretion. G. Sachs, E. Heinz, and K. J. Ullrich, editors, Academic Press, Inc. NY. 165.

Brown, A. C., and K. G. Kastella. 1965. The AC impedance of frog skin and its relation to active transport. *Biophys. J.* 5:591–606.

Clausen, C., and J. M. Fernandez. 1981. A low-cost method for rapid transfer function measurements with direct application to biological impedance analysis. *Pfluegers Arch. Eur. J. Physiol.* 390:290.

Clausen, C., T. E. Machen, and J. M. Diamond. 1982. Changes in cell membranes of bullfrog gastric mucosa with acid secretion. *Science (Wash. D.C.)* 217:448–450.

Clausen, C., S. A. Lewis, and J. M. Diamond. 1979. Impedance analysis of a tight epithelium using a distributed resistance model. *Biophys. J.* 26:291–317.

Clausen, C., and N. K. Wills. 1981. Impedance analysis in epithelia. In Ion Transport by Epithelia. S. G. Schultz, editor. Raven Press, NY. 79–92.

Cole, K. S. 1972. Membrane, Ions, and Impulses. University of California Press, Berkeley, California.

Davson, H. 1964. A Textbook of General Physiology. Little, Brown & Co., Boston. 681.

Diamond, J. M. 1977. The epithelial junction: bridge, gate and fence. *Physiologist.* 20:10–18.

Diamond, J. M., and T. E. Machen. 1983. Impedance analysis in epithelia, and the problem of gastric acid secretion. *J. Membr. Biol.* In press.

Flagg-Newton, J. L., and W. R. Loewenstein. 1980. Asymmetrically permeable membrane channels in cell junction. *Science (Wash. D.C.)* 207:770.

Flemström, G. 1971. Na^+ transport and impedance properties of the isolated frog gastric mucosa at different O_2 tensions. *Biochim. Biophys. Acta.* 225:35–45.

Forte, J. G., J. A. Black, T. M. Forte, T. E. Machen, and J. M. Wolosin. 1982. Ultrastructural changes related to functional activity in gastric oxyntic cells. *Am. J. Physiol.* 241:G349–358.

Forte, J. G., T. M. Forte, and T. K. Ray. 1972. Membranes of the oxyntic cell: their structure, composition, and genesis. *In* Gastric Secretion. G. Sachs, E. Heinz, and K. J. Ullrich, editors, Academic Press, Inc. NY. 37.

Forte, J. G., and T. E. Machen. 1975. Transport and electrical phenomena in resting and secreting piglet gastric mucosa. *J. Physiol. (Lond.).* 224:31–51.

Forte, T. M., T. E. Machen, and J. G. Forte. 1975. Ultrastructural and physiological changes in piglet oxyntic cells during histamine stimulation and metabolic incubation. *Gastroenterology* 69:1208–1222.

Forte, T. M., T. E. Machen, and J. G. Forte. 1977. Ultrastructural changes in oxyntic cells associated with secretory function: a membrane-recycling hypothesis. *Gastroenterology* 73:941–955.

Frömter, E., and J. M. Diamond. 1972. Route of passive ion permeation in epithelia. *Nat. New Biol.* 235:9–13.

Frömter, E., K. Suzuki, G. Kottra, and L. Kampmann. 1981. The paracellular shunt conductance in *Necturus* gallbladder epithelium: comparison of measurements obtained by cable analysis with measurements obtained by a new approach based on intracellular impedance analysis. *In* Epithelial Ion and Water Transport. A. D. C. Macknight and J. P. Leader, editors, Raven Press, NY. 73–83.

Gluck, S., C. Cannon, and Q. Al-Awqati. 1982. Exocytosis regulates urinary acidification in turtle bladder by rapid insertion of H^+ pumps into the luminal membrane. *Proc. Natl. Acad. Sci. USA* 79:4327–4331.

Halliday, D., and R. Resnick. 1967. Physics, Part II. John Wiley & Sons, Inc. NY. 741.

Hamilton, W. C. 1964. Statistics in Physical Science. Ronald Press, NY. 230.

Helander, H. F., S. S. Sanders, W. S. Rehm, and B. I. Hirschowitz. 1972. Quantitative aspects of gastric morphology. *In* Gastric Secretion. G. Sachs, E. Heinz, and K. L. Ullrich, editors. Academic Press, Inc., NY. 69–88.

Hersey, S. J., M. Miller, and D. May. 1982. Pepsinogen secretion by isolated gastric glands. *Fed. Proc.* 41:1498*a*.

Jack, J. J. B., D. Noble, and R. W. Tsien. 1975. Electric Current Flow in Excitable Cells. Clarendon Press, Oxford University Press, Oxford. 25.

Lewis, S. A., and J. M. Diamond. 1976. Na^+ transport by rabbit urinary bladder, a tight epithelium. *J. Membr. Biol.* 28:1–40.

Lewis, S. A., and J. L. C. de Moura. 1982. Incorporation of cytoplasmic vesicles into the apical membrane of mammalian urinary bladder epithelium. *Nature (Lond.).* 297:685–688.

Logsdon, C. D., and T. E. Machen. 1982*a*. Ionic requirements for H^+ secretion and membrane elaboration in frog oxyntic cells. *Am. J. Physiol.* 242:G388–399.

Logsdon, C. D., and T. E. Machen. 1982*b*. Ultrastructural changes during stimulation of amphibian oxyntic cells viewed by scanning and transmission electron microscopy. *Anat. Rec.* 202:73–83.

Machen, T. E., C. Clausen, and J. M. Diamond. 1977. Electrical events during stimulation of HCl secretion by frog gastric mucosa *in vitro*. *Gastroenterology*. 73:970.

Machen, T. E., and J. G. Forte. 1979. Gastric secretion. *In* Membrane Transport in Biology. G. Giebisch, D. C. Tosteson, and H. H. Ussing, editors, Springer-Verlag, Berlin, FRG. Vol. 4B. 693–747.

Machen, T. E., W. Silen, and J. G. Forte. 1978. Na^+ transport by mammalian stomach. *Am. J. Physiol.* 234:E228–235.

Machen, T. E., and T. Zeuthen. 1982. Cl^- transport by gastric mucosa: cellular Cl^- activity and membrane permeability. *Proc. Roy. Soc. Ser. B.* In press.

McLennan, W. L., T. E. Machen, and T. Zeuthen. 1980. Ba^{2+} inhibition of electrogenic Cl^- secretion in *in vitro* frog and piglet gastric mucosa. *Am. J. Physiol.* 239:G151–160.

Noyes, D. H., and W. S. Rehm. 1970. Voltage response of frog gastric mucosa to direct current. *Am. J. Physiol.* 219:184–192.

Rehm, W. S. 1958. Effect of electric current on gastric hydrogen ion and chloride ion secretion. *Am. J. Physiol.* 185:235.

Rehm, W. S., and S. S. Sanders. 1972. Limiting cell membranes of the gastric mucosa and cellular acid-base balance. *In* Gastric Secretion. G. Sachs, E. Heinz, and K. J. Ullrich, editors. Academic Press, Inc., NY. 91.

Rehm, W. S., S. S. Sanders, M. G. Tant, F. M. Hoffman, and J. T. Tarvin. 1976. Conductance of frog gastric mucosa under varying conditions as determined by square-wave analysis. *In* Gastric Hydrogen Secretion. D. K. Kasbekar, G. Sachs, and W. S. Rehm, editors. Marcel Dekker, Inc., NY. 29–53.

Rehm, W. S., and J. T. Tarvin. 1978. Interpretation of the voltage response of epithelial tissue to step currents. *Acta Physiol. Scand. Suppl.* 1978:143–154.

Ring, A., and J. Sandblom. 1980. Impedance of the frog gastric mucosa, the Teorell-Wersäll effect. *Ups. J. Med. Sci.* 85:283–293.

Ruston, H., and J. Bordogna. 1966. *Electric Networks: Functions, Filters, Analysis.* McGraw-Hill, Inc., N.Y. 1–552.

Spenney, J. G., R. G. Shoemaker, and G. Sachs. 1974. Microelectrode studies in fundic gastric mucosa: cellular coupling and shunt conductance. *J. Membr. Biol.* 19:105–128.

Stetson, D. L., S. A. Lewis, W. Alles, and L. B. Wade. 1982. Evaluation by capacitance measurements of antidiuretic hormone-induced membrane area changes in toad bladder. *Biochim. Biophys. Acta.* In press.

Tarvin, J. T., H. A. Helms, J. A. Pirkle, and W. S. Rehm. 1979. Alteration of frog gastric mucosa voltage transients due to the presence of SCN^-. *Biophys. J.* 25:30a.

Teorell, T. 1946. Application of "square wave analysis" to biological studies. *Acta Physiol. Scand.* 12:235–254.

Teorell, T., and R. Wersäll. 1945. Electrical impedance properties of surviving gastric mucosa of the frog. *Acta Physiol. Scand.* 10:243–257.

Wade, J. B., D. L. Stetson, and S. A. Lewis. 1981. ADH action: evidence for a membrane shuttle mechanism. *Ann. N.Y. Acad. Sci.* 372:106–117.

Wright, G. H. 1974. Electrical impedance, ultrastructure and ion transport in foetal gastric mucosa. *J. Physiol. (Lond.).* 242:661–672.